First-principles study of crystal structural stability and electronic and magnetic properties in $LaMn_7O_{12}$

2010 J. Phys.: Condens. Matter 22 246001

(http://iopscience.iop.org/0953-8984/22/24/246001)

J. Phys.: Condens. Matter **22** (2010) 246001 (8pp) doi:10.1088/0953-8984/22/24/246001

First-principles study of crystal structural stability and electronic and magnetic properties in $LaMn_7O_{12}$

X J Liu[1,2], S H Lv[2,3], E Pan[1,5], J Meng[2,6] and J D Albrecht[4]

[1] Computer Modeling and Simulation Group, College of Engineering, University of Akron, OH 44325-3905, USA
[2] State Key Laboratory of Rare Earth Resources Utilization, Changchun Institute of Applied Chemistry, Chinese Academy of Sciences, Changchun, Jilin 130022, People's Republic of China
[3] Graduate School, Chinese Academy of Sciences, Beijing 100049, People's Republic of China
[4] Air Force Research Laboratory, Wright-Patterson Air Force Base, OH 45433, USA

E-mail: pan2@uakron.edu and jmeng@ciac.jl.cn

Received 2 February 2010, in final form 3 May 2010
Published 1 June 2010
Online at stacks.iop.org/JPhysCM/22/246001

Abstract

The crystal structure, electronic and magnetic properties of $LaMn_7O_{12}$ ($(LaMn_3^{3+})_A Mn_4^{3+}O_{12}$) are investigated by GGA (LSDA) and GGA + U (LSDA + U) ($0.0 \leqslant U \leqslant 5.0$ eV) methods. Based on two experimentally refined structures (distinguished by the distortion parameter Δ, namely $\mathbf{S}_{\mathrm{I}}$ ($\Delta = 8.5 \times 10^{-5}$) and $\mathbf{S}_{\mathrm{II}}$ ($\Delta = 25.0 \times 10^{-4}$)), GGA and GGA + U with $U < 3.0$ eV calculations indicate that $\mathbf{S}_{\mathrm{I}}$ with a small distortion is the lowest-energy crystal structure while GGA + U with $3.0 \leqslant U \leqslant 5.0$ eV calculations show that $\mathbf{S}_{\mathrm{II}}$ with a larger distortion is the ground-state crystal structure. Within the LSDA method, $\mathbf{S}_{\mathrm{II}}$ is always the ground-state structure no matter if U is considered or not. There are two independent magnetic sublattices: Mn^{3+} within the A site and Mn^{3+} within the B site. First, it is predicted that A-site Mn^{3+} ions are preferably AFM-coupled in G-type (antiferromagnetically coupled in three directions). Based on this result, four magnetic configurations (**FM**-$A^{\uparrow\uparrow}B^{\uparrow\uparrow}$, **AFM1**-$A^{\uparrow\uparrow}B^{\downarrow\downarrow}$, **AFM2**-$A^{\uparrow\downarrow}B^{\uparrow\uparrow}$ and **AFM3**-$A^{\uparrow\downarrow}B^{\uparrow\downarrow}$) are designed, and their total energies are calculated. Our results demonstrate that **AFM2** and **AFM3** are the lowest magnetic state, respectively, for $\mathbf{S}_{\mathrm{I}}$ and $\mathbf{S}_{\mathrm{II}}$. Correspondingly, $LaMn_7O_{12}$ is metallic with no orbital ordering at **AFM2** for $\mathbf{S}_{\mathrm{I}}$ while it is an insulator with orbital ordering at **AFM3** for $\mathbf{S}_{\mathrm{II}}$. Thus, modulation of the distortion parameter Δ, e.g. by chemical doping, could be employed as a new avenue to induce a magnetic phase transition and the corresponding metal-to-insulator transition in $LaMn_7O_{12}$.

(Some figures in this article are in colour only in the electronic version)

1. Introduction

Spin, charge, orbital and lattice degrees of freedom play important roles in the electronic, magnetic and transport properties of transition metal oxides [1–6]. On explaining these couplings, Goodenough [7] showed that the dominant role of the Anderson superexchange interaction [8] between neighboring Mn ions was through the Mn–O–Mn path of the corner-sharing network of MnO_6 octahedra. The Goodenough–Kanamori–Anderson (GKA) rules [7, 9, 10] provide a model to describe the strength and orientation of the magnetic interaction, in which the key parameters are the Mn–O–Mn bond angles and the Mn–O bond length. It is demonstrated that the stabilization of a given charge, magnetic and orbital orderings requires a well-defined pattern of the cooperative buckling and distortion of the octahedral network.

[5] Address for correspondence: Computer Modeling and Simulation Group, University of Akron, 302 Buchtel Common, Akron, OH 44325, USA.
[6] Address for correspondence: The State Key Laboratory of Rare Earth Resource Utilization, Changchun Institute of Applied Chemistry, CAS, 5625 Renmin Street, Changchun, Jilin 130022, People's Republic of China.

In order to validate the GKA rules, Prodi *et al* synthesized single crystals of $LaMn_7O_{12}$ under high pressure at $P = 4$ GPa and high temperature $T = 1000\,^{\circ}C$ [11]. $LaMn_7O_{12}$ belongs to the $A'A_3B_4O_{12}$-type double perovskites, which have received wide attention owing to their special ordered structures and a variety of physical properties [12–18]. In $LaMn_7O_{12}$ there are only Mn^{3+}, thus only magnetic and orbital orderings need to be considered, excluding the charge ordering effect. Their crystal structure is refined to the monoclinic $I2/m$ space group. As for their magnetic property, it is found that there exist two transition temperatures: $T_{N,B} = 78$ K due to the C-type antiferromagnetic (AFM) structure within B-site Mn^{3+} ions and $T_{N,A} = 21$ K due to a second AFM structure within A-site Mn^{3+} ions.

Actually in 1974, Bochu *et al* also successfully refined the structure of $LaMn_7O_{12}$ in the monoclinic $I2/m$ space group [19]. Detailed comparison between these two experimentally refined structures reveals that they show remarkable differences, especially for the bond length differences around the two B-site Mn ions (which will be shown below). Since it is believed that in $LaMn_7O_{12}$ the existence of distinct Jahn–Teller (JT) B-site Mn ions plays a primary role in determining the magnetic coupling, we suspect that different distortions around the B-site Mn ions should quantitatively, and even qualitatively, influence their magnetic properties and then the corresponding electronic properties.

It is well known that in transition metal oxides strong local Coulomb interactions play very important roles, and are responsible for the observed ground states and the associated physical properties. For instance, the electronic interactions could suppress charge fluctuations in Mott insulators and lead to rather strong coupling among spin, charge, orbital and lattice degrees of freedom [20]. Thus the standard density-functional theory (DFT) often fails to reproduce the observed electronic structure and magnetic properties. Indeed, two distinct ground states with either checkerboard charge ordering or Zener polaron formation were reported, depending on the proportion of Hartree–Fock exchange used in $La_{0.5}Ca_{0.5}MnO_3$ [21]. Similarly, the charge-orbital ordering and hence the Verwey metal–insulator transition was shown to be driven by the on-site Fe d-electron correlation in Fe_3O_4 [22].

Therefore, it becomes necessary that in the study of $LaMn_7O_{12}$ the following three key issues be resolved: (i) which is the most stable structure for the two experimentally refined $I2/m$ crystal structures; (ii) how the different Jahn–Teller distortions within B-site Mn^{3+} ions affect their magnetic interactions and electronic structures and (iii) how the Coulomb interaction affects its structural stability and electronic and magnetic properties. Besides our studies on these three issues, we will also present a detailed investigation on the magnetic coupling within A-site Mn^{3+} ions since in $LaMn_7O_{12}$ there exists a second sublattice of JT Mn^{3+} ions in A sites with a square coordination.

2. Crystal structure and magnetic orders

$LaMn_7O_{12}$ is refined in the monoclinic $I2/m$ space group. It is a pseudocubic perovskite-like structure which belongs to the family of quadruple perovskites with general formula $A'A_3B_4O_{12}$, where A′ can be a nonmagnetic monovalent, divalent or trivalent cation, and A and B are the JT ions. In $LaMn_7O_{12}$, both the A and B sites are occupied by Mn^{3+} ions, resulting in two interpenetrating sublattices of JT ions with octahedral (B-site Mn^{3+}) and square-planar (A-site Mn^{3+}) coordination (figures 1(a) and (b)). Figure 1(b) shows that the monoclinic distortion splits the pristine eightfold B site into two fourfold 4e and 4f sites and the pristine sixfold A sites into three twofold sites (A1, A2 and A3) with $2/m$ point symmetry. The refined crystal parameters and Mn–O bond length of the B sites by Bochu [19] (designated as $\mathbf{S}_I$) and Prodi [11] (designated as $\mathbf{S}_{II}$) are listed in table 1. From table 1, we see that the bond length differences around 4e and 4f are larger in $\mathbf{S}_{II}$ than those in $\mathbf{S}_I$. For example, in $\mathbf{S}_{II}$ the bond length differences are 0.25 Å and 0.23 Å around 4e and 4f, respectively, while they are only 0.04 Å and 0.03 Å in $\mathbf{S}_I$. The distortion parameter Δ has been used to characterize the JT distortion around the JT ions [23] and it is defined as $\Delta = (1/N)\sum_{n=1,N}\{(d_n - \langle d\rangle)/\langle d\rangle\}^2$ in which $\langle d\rangle$ is the average Mn–O bond distance. Based on this formula, the distortion parameter (Δ) is found to be 5.8×10^{-5} and 24.0×10^{-4}, respectively, for $\mathbf{S}_I$ and $\mathbf{S}_{II}$, an order-of-magnitude difference.

Table 1. Crystal parameters and selected bond lengths (in ångströms) for $LaMn_7O_{12}$ by Bochu *et al* [19] ($\mathbf{S}_I$) and Prodi *et al* [11] ($\mathbf{S}_{II}$). Δ is used to characterize the distortion which is defined as $\Delta = (1/N)\sum_{n=1,N}\{(d_n - \langle d\rangle)/\langle d\rangle\}^2$. The energy differences (meV) between different magnetic configurations taking **FM** as reference obtained using GGA + U with U equal to 3.0 and 4.0 eV.

	$I2/m$—$\mathbf{S}_I$	$I2/m$—$\mathbf{S}_{II}$
Crystal parameters		
a (Å)	7.516	7.509
b (Å)	7.376	7.349
c (Å)	7.516	7.504
β (deg)	91.30	91.354
Bond length Å		
Mn_{4e}–O_1	2.012	2.145
Mn_{4e}–O_3	1.991	1.968
Mn_{4e}–O_4	1.967	1.908
Δ_{4e}	8.5×10^{-5}	25.0×10^{-4}
Mn_{4f}–O_2	1.990	1.890
Mn_{4f}–O_3	1.973	1.987
Mn_{4f}–O_4	2.010	2.129
Δ_{4f}	5.8×10^{-5}	24.0×10^{-4}
GGA + U (3.0 eV) calculated results (meV)		
$A^{\uparrow\uparrow}B^{\uparrow\uparrow}$ (**FM**)	0.0	0.0
$A^{\uparrow\uparrow}B^{\downarrow\downarrow}$ (**AFM1**)	−34	−45
$A^{\uparrow\downarrow}B^{\uparrow\uparrow}$ **A-AFM2**	−435	−211
(**AFM2**) **G-AFM2**	−474	−246
$A^{\uparrow\downarrow}B^{\uparrow\downarrow}$ (**AFM3**)	−260	−526
GGA + U (4.0 eV) calculated results (meV)		
$A^{\uparrow\uparrow}B^{\uparrow\uparrow}$ (**FM**)	0.0	0.0
$A^{\uparrow\uparrow}B^{\downarrow\downarrow}$ (**AFM1**)	−57	−59
$A^{\uparrow\downarrow}B^{\uparrow\uparrow}$ **A-AFM2**	−542	−239
(**AFM2**) **G-AFM2**	−576	−275
$A^{\uparrow\downarrow}B^{\uparrow\downarrow}$ (**AFM3**)	−278	−587

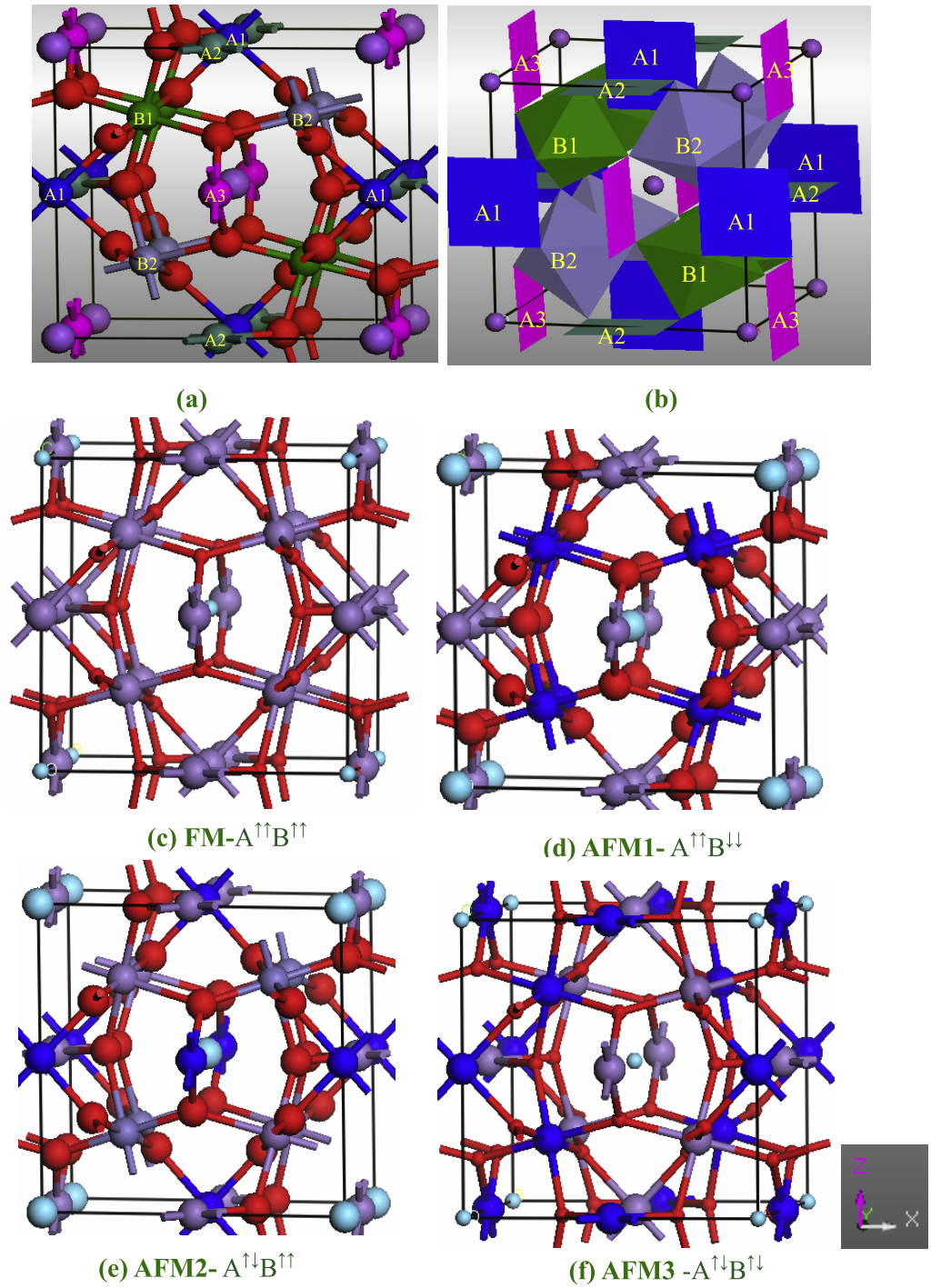

Figure 1. (a) Crystal structures of $LaMn_7O_{12}$ in $I2/m$ monoclinic space group and (b) its monoclinic distortion splitting the B-site Mn ions into B1 (4e) and B2 (4f) sites and A-site Mn ions into A1, A2 and A3. (c)–(f) Present the four designed magnetic configurations (**FM**, **AFM1**, **AFM2** and **AFM3**, respectively) with purple (gray) denoting the spin-up direction and blue (black) the spin-down direction.

Thus by comparative study of their magnetic and electronic properties on these two structures, the delicate interaction between the structural distortion and spin/orbital orderings in this compound can be investigated.

There exist two magnetic sublattices (A and B) in this compound. It was found experimentally that their orderings occurred independently from each other and that their magnetic structure of the B sublattice turned out to be of the C type (i.e. *antiferromagnetically* coupled to the *ferromagnetic ac* plane). In order to study the magnetic couplings, *four* magnetic configurations are taken into account: (1) **FM** ($A^{\uparrow\uparrow}B^{\uparrow\uparrow}$) where the Mn ions are ferromagnetically coupled within A and B sites, respectively, and they are also ferromagnetically coupled between A and B sites (figure 1(c)); (2) **AFM1** ($A^{\uparrow\uparrow}B^{\downarrow\downarrow}$) where the Mn ions are ferromagnetically coupled within A and B sites, respectively, but they are antiferromagnetically coupled between A and B sites (figure 1(d)); (3) **AFM2** ($A^{\uparrow\downarrow}B^{\downarrow\downarrow}$) where the Mn ions are antiferromagnetically coupled

within A sites and ferromagnetically coupled within B sites (figure 1(e)) and (4) **AFM3** ($A^{\uparrow\downarrow}B^{\uparrow\downarrow}$) where the Mn ions are antiferromagnetically coupled within A and B sites, respectively, and also antiferromagnetically coupled between A and B sites (figure 1(f)). In addition, in order to find which AFM configuration has the lowest energy within A-site Mn^{3+}, based on the designed **AFM2** configuration, we arranged the A-site Mn^{3+} in A-type AFM (designated as **A-AFM2**), as tentatively determined experimentally [11] and G-type AFM (designated as **G-AFM2**) as determined from its isostructural compound $NaMn_7O_{12}$ [24].

3. Computational details

All calculations in this paper are carried out using the highly accurate full-potential linearized augmented plane wave plus local orbitals (FP-LAPW + lo) method [25, 26] with density-functional theory implemented in the WIEN2K package [27, 28]. In this method, the space is divided into an interstitial region and the nonoverlapping muffin-tin (MT) spheres are centered at the atomic sites. In the MT region, the basis sets are described by radial solutions of the one-particle Schrödinger equation (at fixed energy) and their energy derivatives are multiplied by spherical harmonics.

In order to achieve energy convergence, the wavefunctions in the interstitial region are expanded in plane waves with a cutoff $R_{\mathrm{MT}}^{\mathrm{min}} K_{\mathrm{max}} = 7$, where $R_{\mathrm{MT}}^{\mathrm{min}}$ denotes the smallest atomic sphere radius and K_{max} the magnitude of the largest K vector in the plane wave expansion. The values of the atomic sphere radii (R_{MT}) are taken as 2.50, 1.88 and 1.68 au for La, Mn and O, respectively. For the electron population analysis, the muffin-tin radii (R_{MT}) are chosen to be the touching spheres to keep as much core charges inside the muffin tin as possible. The valence wavefunction inside the spheres is expanded up to $l_{\mathrm{max}} = 10$, while the charge density in terms of the Fourier series is expanded up to $G_{\mathrm{max}} = 12$. The total Brillouin zone is sampled with 1000 k-points. The Brillouin zone integration is carried out with a modified tetrahedron method [29]. The self-consistent field is considered to be achieved when the total energy difference between succeeding iterations is less than 10^{-5} Ryd.

As for the exchange–correlation potential, we employ both the standard generalized gradient approximation (GGA) using the Perdew–Burke–Ernzerhof scheme [30] and the local spin density approximation (LSDA) using Cerply-Alder. In addition, to properly describe the strong electron correlation in the Mn^{3+} 3d orbitals, the GGA plus on-site repulsion U method (GGA + U and LSDA + U) is also used [31–33] with effective U values ($U_{\mathrm{eff}} = U - J$) of 0.0–5.0 eV for Mn. Unless otherwise indicated, the reported results are based on GGA + U_{eff} (with $U_{\mathrm{eff}} = 4.0$ eV for Mn).

4. Results and analyses

4.1. Magnetic coupling within A-site Mn^{3+}

We first consider the magnetic structure of Mn^{3+} within the A sublattice. The topology of this sublattice differs from that of the B sublattice, as seen from figure 1(b). The nearest neighbors of each Mn are four, instead of six, and form a square within the plane of the ions, instead of an octahedron. According to the neutron data, Prodi *et al* tentatively designated the A-type AFM configuration within this sublattice [11]. However, we noticed that, in $NaMn_7O_{12}$, which is also in the same $I2/m$ space group, the A-site Mn ions were believed to be the G-type AFM [24]. Hence, we calculated the energies of both **A-AFM2** and **G-AFM2** as defined above in which the A-site Mn^{3+} ions are in an A-type and G-type AFM arrangement, respectively. It is observed from table 1 that for both $\mathbf{S}_{\mathrm{I}}$ and $\mathbf{S}_{\mathrm{II}}$, the energy of the G-type AFM arrangement is always lower by about 35 meV than that of the A-type. Thus in the following analysis, the AFM coupling of A-site Mn^{3+} is referred to the G-type AFM.

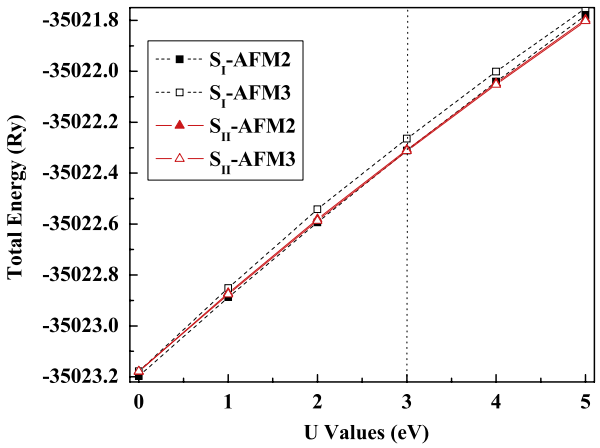

Figure 2. Variation of the total energies of $\mathbf{S}_{\mathrm{I}}$ and $\mathbf{S}_{\mathrm{II}}$ at **AFM2** and **AFM3** magnetic configurations versus different U values.

4.2. Electronic correlation effect on crystal structure and magnetic property

Figure 2 shows the variation of the total energies of **AFM2** (solid) and **AFM3** (empty) in both $\mathbf{S}_{\mathrm{I}}$ (square) and $\mathbf{S}_{\mathrm{II}}$ (triangle) structures versus the U values based on the GGA + U method. It is obvious that, when $U < 3.0$ eV, $\mathbf{S}_{\mathrm{I}}$ is the lowest-energy crystal structure, while when $U \geqslant 3.0$ eV, $\mathbf{S}_{\mathrm{II}}$ becomes the ground-state crystal structure. Similar results were also obtained in $La_{0.5}Ca_{0.5}MnO_3$ using the hybrid Hartree–Fock/density-functional theory *ab initio* method [21]. It was found that the ground-state charge ordering of $La_{0.5}Ca_{0.5}MnO_3$ could switch between checkerboard charge ordering and a Zener polaron one if the percentage of Hartree–Fock (HF) exchange was varied. These two states are therefore similar in energy and the actual ground state might depend on the specific A (La) and B (Mn) ions or even sample preparation, history and ambient conditions. In our calculation, an increase in U could be viewed as the increase of the percentage in HF exchange, and thus different ground-state crystal structures are also obtained with different U values. We consider that the different crystal structures obtained by Prodi *et al* [11] and Bochu *et al* [19] might be due to the different sample preparation and ambient conditions. Within the LSDA calculation, $\mathbf{S}_{\mathrm{II}}$ is the ground-state crystal structure, and when

Table 2. LSDA calculated total energy differences (meV) between different magnetic configurations taking the FM state of $\mathbf{S}_{\mathrm{I}}$ as a reference.

	$I2/m$—$\mathbf{S}_{\mathrm{I}}$	$I2/m$—$\mathbf{S}_{\mathrm{II}}$
LSDA		
$A^{\uparrow\uparrow}B^{\uparrow\uparrow}$ (**FM**)	0.0	195
$A^{\uparrow\uparrow}B^{\downarrow\downarrow}$ (**AFM1**)	−107	−235
$A^{\uparrow\downarrow}B^{\uparrow\uparrow}$ (**AFM2**)	−559	−421
$A^{\uparrow\downarrow}B^{\uparrow\downarrow}$ (**AFM3**)	−211	−596

the electronic correlation (U) is considered, $\mathbf{S}_{\mathrm{II}}$ is more stable due to the larger energy difference between $\mathbf{S}_{\mathrm{I}}$ and $\mathbf{S}_{\mathrm{II}}$.

We have also calculated the total energies for the four magnetic configurations of both $\mathbf{S}_{\mathrm{I}}$ and $\mathbf{S}_{\mathrm{II}}$ structures with results listed in table 1 based on GGA + U and in table 2 based on LSDA. It is clearly observed that, based on both GGA + U and LSDA, the two different structural distortions ($\mathbf{S}_{\mathrm{I}}$ and $\mathbf{S}_{\mathrm{II}}$) lead to completely different magnetic interactions within B sites. Mn_{4e} and Mn_{4f} are likely to be AFM-coupled in $\mathbf{S}_{\mathrm{II}}$ whilst they are favorable to be FM-coupled in $\mathbf{S}_{\mathrm{I}}$. Thus, the lowest-energy magnetic configurations is **AFM2** for $\mathbf{S}_{\mathrm{I}}$, in which the B-site Mn ions are FM-coupled whilst the A-site Mn ions are AFM-coupled, and **AFM3** for $\mathbf{S}_{\mathrm{II}}$, in which both B-site and A-site Mn ions are AFM-coupled. Our calculated prediction in $\mathbf{S}_{\mathrm{II}}$, where the two B-site Mn ions turn out to be AFM-coupled, is consistent with the experimental result by Prodi *et al* [11].

In figures 3(a) and (b), we present the total electronic density of states (TDOS) obtained by both the GGA (top row) and GGA + U (bottom row) methods for the **AFM2** configuration in $\mathbf{S}_{\mathrm{I}}$ and **AFM3** in $\mathbf{S}_{\mathrm{II}}$, respectively. For $\mathbf{S}_{\mathrm{I}}$, both the GGA (LSDA) and GGA + U (LSDA + U) calculations predict a half-metallic character in its lowest-energy magnetic configuration **AFM2**, with a metallic character for the spin-up channel and semiconductor behavior for the spin-down (figure 3(a)). For **AFM3** configuration in $\mathbf{S}_{\mathrm{II}}$, GGA (LSDA) calculation shows a metallic character for $LaMn_7O_{12}$ (figure 3(b), top row), contrary to the insulator behavior experimentally determined. This indicates that the standard GGA (LSDA) calculation is unable to describe properly the electronic structure due to the strongly correlated nature of electrons in this material. The GGA + U (LSDA + U) method, on the other hand, is able to predict a clear insulator character, as shown in figure 3(b) in the bottom row with a gap of about 1.0 eV, compared to the experimental value of 0.22 eV. While the lower experimental bandgap could be due to the existence of midgap defect states which might be difficult to measure, our further calculation indicates that, with U varying from 1.0 to 5.0 eV, the energy gap changes from 0.20 to 3.0 eV. Therefore, a reliable measurement of the gap is needed in order to confirm the proper U values for this system.

In order to investigate the relationship between the magnetic coupling and electronic structure, we have also carried out the calculations for the **AFM3** magnetic configuration in $\mathbf{S}_{\mathrm{I}}$, with the result shown in figure 3(c). It is clear that $LaMn_7O_{12}$ also exhibits an insulator property in the assumed **AFM3** magnetic state in the $\mathbf{S}_{\mathrm{I}}$ structure using the GGA + U (LSDA + U) method. These results indicate that, in $LaMn_7O_{12}$, its local structure distortion within B-site Mn ions and the magnetic coupling behavior (AFM or FM) are delicately correlated. External pressure and/or chemical doping, which will change the distortion within B-site ions (e.g. substitution of La by other rare earth elements), could induce a magnetic phase transition within B-site Mn ions.

4.3. Electronic structure analysis

We then investigate the relationship between the magnetic property and electronic structures in this compound based on the GGA + U calculation. The site- and angular-projected partial density of states (PDOS) for Mn_{4e} and Mn_{4f} of **AFM2** in $\mathbf{S}_{\mathrm{I}}$ and **AFM3** in $\mathbf{S}_{\mathrm{II}}$ are shown in figures 4(a) and (b), respectively. The Mn^{3+} ion in $LaMn_7O_{12}$ is in a $3d^4$ configuration. In an octahedral crystal field, the Mn 3d orbitals will split into three lower t_{2g} and two upper e_g orbitals. However, because of the distorted octahedron as shown in figure 1(b) and table 1, the orbitals are further split. Thus three of the four electrons occupy the three t_{2g} orbitals whilst the remained fourth electron occupies the lower e_g orbital. In $LaMn_7O_{12}$, the two B-site Mn^{3+} ions at the 4e and 4f sites possess distinct JT distorted octahedra, so the fourth electron should prefer different e_g orbitals, resulting in orbital ordering in this compound. In more detail, in $\mathbf{S}_{\mathrm{II}}$ as shown in figure 4(b), the t_{2g} orbitals (i.e. d_{xy}, d_{xz} and d_{yz}) in both Mn_{4e} and Mn_{4f} are occupied. Recalling the data in table 1 where the bond Mn_{4e}–O_4 (along the z direction) is the longest (2.1446 Å) and Mn_{4f}–O_4 is the shortest (1.8903 Å) for $\mathbf{S}_{\mathrm{II}}$, this distinct structural distortion would certainly lead to a different electron occupation for the fourth electron. The angular-PDOS shows that the fourth electron occupies the d_z^2 orbital on Mn_{4e} while it occupies the $d_{x^2-y^2}$ orbital on Mn_{4f}, which is consistent with their local structure distortion. For $\mathbf{S}_{\mathrm{I}}$, the site- and angular-PDOS, as plotted in figure 4(a) for its lowest-energy magnetic state **AFM2**, show that the fourth electron occupies almost equally the d_{z^2} and $d_{x^2-y^2}$ orbitals; thus there is no orbital ordering for $\mathbf{S}_{\mathrm{I}}$. In order to explicitly indicate different orbital orderings in these two different structures, figures 5(a) and (b) show the contour plots around the Fermi level. From these figures, one can clearly see that, for $\mathbf{S}_{\mathrm{II}}$ in the **AFM3** state, orbital ordering forms while for $\mathbf{S}_{\mathrm{I}}$ in the **AFM2** state, orbital ordering disappears. However, in the **AFM3** magnetic configuration of $\mathbf{S}_{\mathrm{I}}$, similar PDOS analysis (figure 4(c)) shows that there also exists orbital ordering as observed in $\mathbf{S}_{\mathrm{II}}$, although their ordering is not very complete due to the comparatively small exchange split caused by a smaller distortion. These analyses indicate that, in $LaMn_7O_{12}$, magnetic coupling determines the existence of the orbital ordering, which is consistent with the GKA rules. In the GKA rules, the strength and orientation of the magnetic interaction are described and especially it provides the frame of the Jahn–Teller-driven polarization of the two relevant e_g $d_{x^2-y^2}$ and d_{z^2} orbitals in the MnO_6 octahedron. Comparison of the two structures $\mathbf{S}_{\mathrm{I}}$ and $\mathbf{S}_{\mathrm{II}}$, their difference is mainly in the bond length differences (Δ). However, local structural distortion leads to different occupation ($d_{x^2-y^2}$ or d_{z^2}) of the fourth electron in the octahedral Mn ions, which is closely relevant to the magnetic ordering.

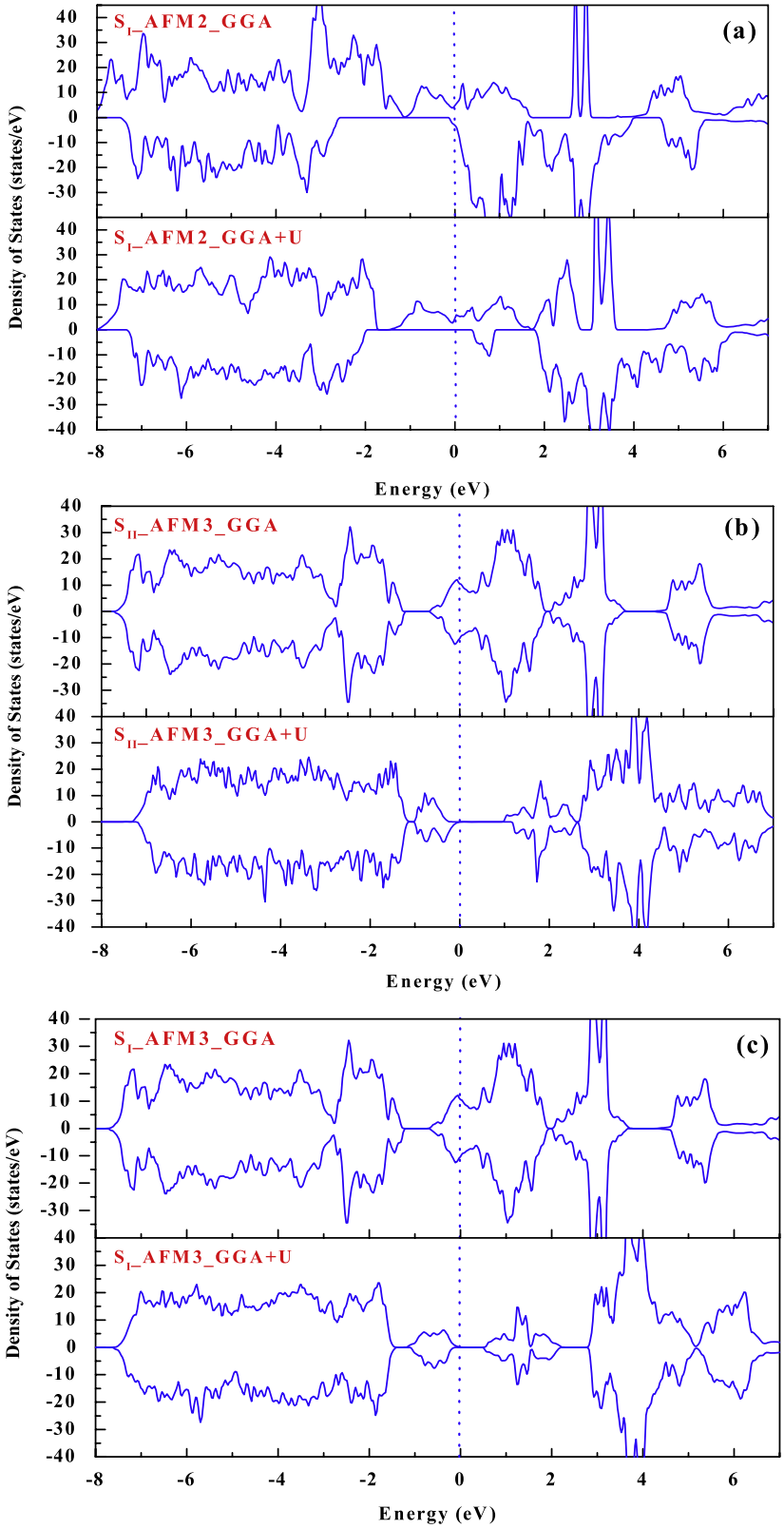

Figure 3. Total density of states for $\mathbf{S_I}$ in **AFM2** magnetic state (a), $\mathbf{S_{II}}$ in **AFM3** magnetic state (b) and $\mathbf{S_I}$ in **AFM3** magnetic state (c) obtained by both GGA (top) and GGA + U (bottom) methods.

5. Conclusions

We have investigated the structural stability, electronic and magnetic properties of $LaMn_7O_{12}$ and the electronic correlation effects on these properties by using GGA (LSDA) and GGA + U (LSDA + U) methods. Our results indicate clearly that the distortion (mainly the bond length difference) could significantly influence the magnetic and electronic

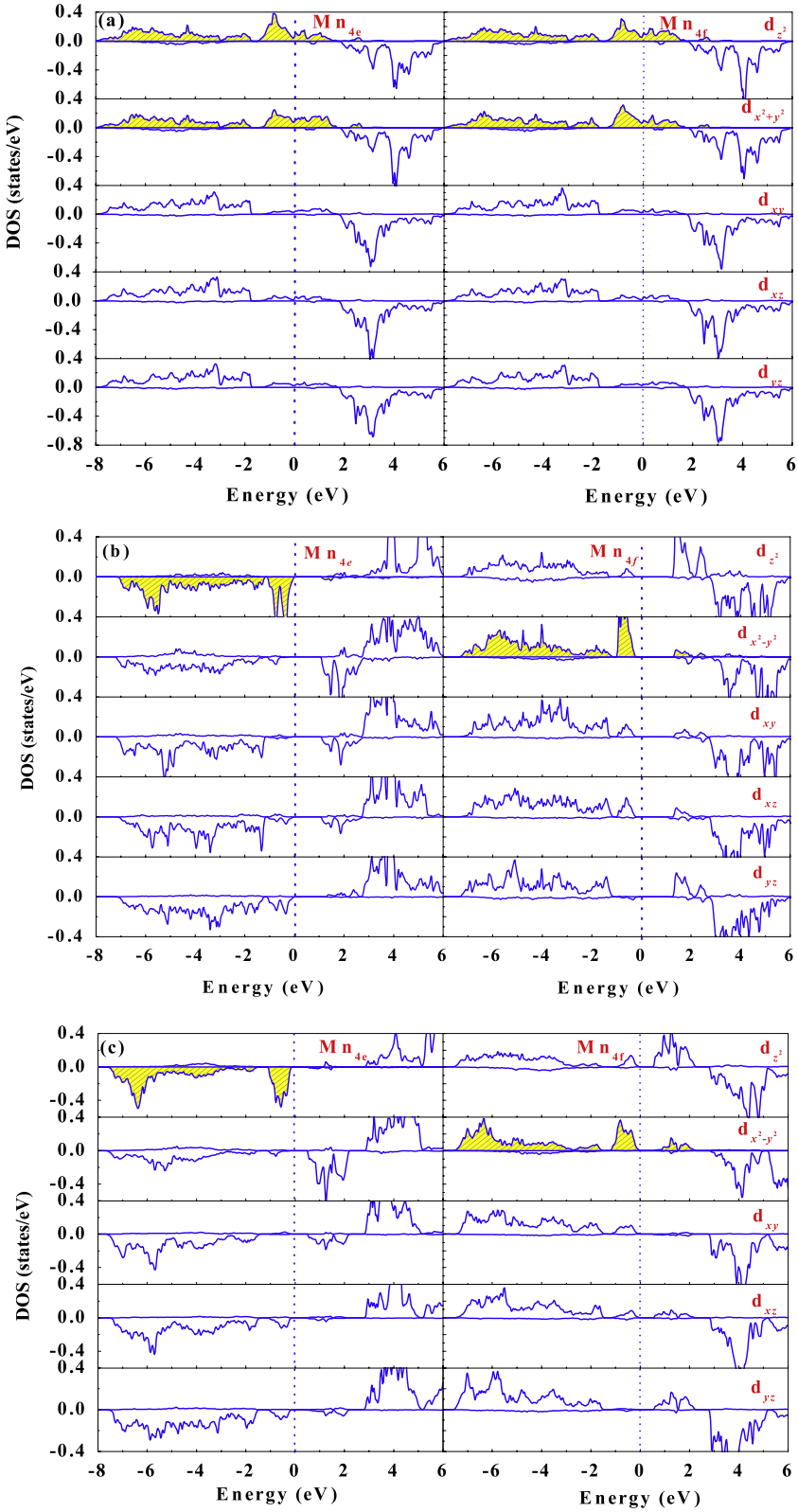

Figure 4. Partial density of states of the two B-site Mn ions (Mn_{4e} left and Mn_{4f} right) for $\mathbf{S}_{\mathrm{I}}$ in the **AFM2** state (a), $\mathbf{S}_{\mathrm{II}}$ in the **AFM3** state (b) and $\mathbf{S}_{\mathrm{I}}$ in the **AFM3** state (c) obtained by the GGA + U ($U_{\mathrm{eff}} = 4.0$ eV) method.

properties and orbital ordering in the quadruple perovskite compound $LaMn_7O_{12}$. Total energy calculations for the four designed magnetic configurations of the two experimental structures show that in $\mathbf{S}_{\mathrm{I}}$, where Mn^{3+} ions have a small bond length difference within B sites, the coupling is prone to be FM and that in $\mathbf{S}_{\mathrm{II}}$, where there is a large bond length difference within B-site Mn ions, the coupling is inclined to be AFM. Furthermore, the AFM coupling leads to an insulator behavior

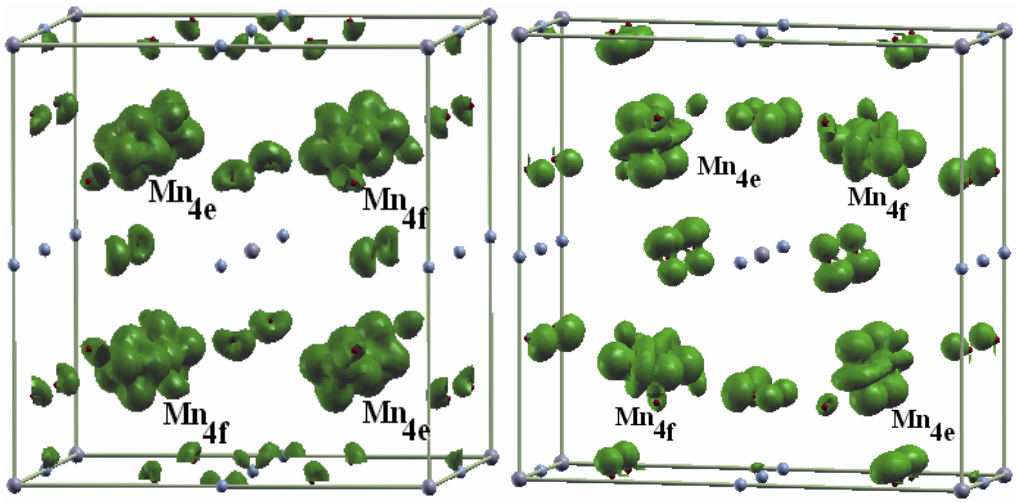

Figure 5. Spin density plot (isosurface at 0.3 e Å^{-3}, mapped by XcrySDen) within the energy interval around −1.0–0.0 eV from GGA + U ($U_{\rm eff}$ = 4.0 eV) calculation in their lowest-energy magnetic states: $\mathbf{S}_{\rm I}$ in **AFM2** (a) and $\mathbf{S}_{\rm II}$ in **AFM3** (b).

and a clear orbital ordering of d_{z^2} and $d_{x^2-y^2}$ in the $\mathbf{S}_{\rm II}$ structure while the FM coupling induces a metallic character with no orbital ordering in the $\mathbf{S}_{\rm I}$ structure. For the A-sublattice Mn ions, the G-type AFM configuration is the lower energy state. Our GGA + U (LSDA + U) calculations further indicate that in $LaMn_7O_{12}$ the on-site Coulomb repulsion plays an important role in its crystal structure, electronic property and orbital ordering.

Acknowledgments

This work was partially supported by the National Natural Science Foundation of China through grant nos. 20831004, 20671088 and 20601026, and by AFOSR FA9550-06-1-0317.

References

[1] Kugel K I and Khomskii D I 1973 *Sov. Phys.—JETP* **37** 725
Kugel K I and Khomskii D I 1982 *Sov. Phys.—Usp.* **25** 231
[2] Tokura Y and Nagaosa N 2000 *Science* **288** 462
[3] Edwards A J and Peacock R D 1959 *J. Chem. Soc.* 4126
Scatturin V, Corliss L, Elliott N and Hastings J 1961 *Acta Crystallogr.* **14** 19
Yoneyama S and Hirakawa K 1966 *J. Phys. Soc. Japan* **21** 183
[4] Margadonna S and Karotsis G 2006 *J. Am. Chem. Soc.* **128** 16436
[5] Okimoto Y, Katsufuji T, Ishikawa T, Urushibara A, Arima T and Tokura Y 1995 *Phys. Rev. Lett.* **75** 109
[6] Radaelli P G, Cox D E, Marezio M and Cheong S W 1997 *Phys. Rev.* B **55** 3015
[7] Goodenough J B 1963 *Magnetism and Chemical Bond* (New York: Interscience)
[8] Anderson P W 1959 *Phys. Rev.* **115** 2
[9] Kanamori J 1959 *J. Phys. Chem. Solids* **10** 87
[10] Anderson P W 1963 *Solid State Physics* vol 14, ed F Seits and D Tumbull (New York: Academic) p 99
[11] Prodi A, Gilioli D, Cabassi R, Bolzoni F, Licci F, Huang Q Z, Lynn J W, Affronte M, Gauzzi A and Marezio M 2009 *Phys. Rev.* B **79** 085105
[12] Long Y W, Saito T, Tohyama T, Oka K, Azuma M and Shimakawa Y 2009 *Inorg. Chem.* **48** 8489
[13] Long Y W, Hayashi N, Saito T, Azuma M, Muranaka S and Shimakawa Y 2009 *Nature* **458** 60
[14] Shimakawa Y 2008 *Inorg. Chem.* **47** 8562
[15] Imamura N, Karppinen M, Motohashi T, Fu D S, Itoh M and Yamauchi H 2008 *J. Am. Soc. Chem.* **130** 14948
[16] Shiraki H, Saito T and Shimakawa Y 2008 *Chem. Mater.* **20** 7077
[17] Yamada I, Takata K, Hayashi N, Shinohara S, Azuma M, Mori S, Muranaka S, Shimakawa Y and Takano M 2008 *Angew. Chem. Int. Edn* **47** 7032
[18] Mizumaki M, Saito T, Shiraki H and Shimakawa Y 2009 *Inorg. Chem.* **48** 3499
[19] Bochu B, Chenavas J, Joubert J C and Marezio M 1974 *J. Solid State Chem.* **11** 88
[20] Imada M, Fujimori A and Tokura Y 1998 *Rev. Mod. Phys.* **70** 1039
[21] Patterson C H 2005 *Phys. Rev.* B **72** 085125
[22] Jeng H T, Guo G Y and Huang D J 2006 *Phys. Rev.* B **74** 195115
[23] Rodríguez-Carvajal J, Hennion M, Moussa F, Moudden A H, Pinsard L and Revcolevschi A 1998 *Phys. Rev.* B **57** R3189
[24] Prodi A, Gilioli E, Gauzzi A, Licci F, Marezio F M, Bolzoni F, Huang Q, Santoro A and Lynn J W 2004 *Nat. Mater.* **3** 48
[25] Sjöstedt E, Nordström L and Singh D J 2000 *Solid State Commun.* **114** 15
[26] Madsen G K H, Blaha P, Schwarz K, Sjöstedt E and Nordström L 2001 *Phys. Rev.* B **64** 195134
[27] Schwarz K and Blaha P 2003 *Comput. Mater. Sci.* **28** 259
[28] Blaha P, Schwarz K, Madsen G K H, Kvasnicka D and Luitz L 2001 *WIEN2k, An Augmented Plane Wave Plus Local Orbitals Program for Calculating Crystal Properties* (Austria: Vienna University of Technology)
[29] Blöchl P E 1994 *Phys. Rev.* B **50** 17953
[30] Perdew J P, Burke K and Ernzerhof M 1996 *Phys. Rev. Lett.* **77** 3865
[31] Liechtenstein A I, Anisimov V I and Zaanen J 1995 *Phys. Rev.* B **52** R5467
[32] Anisimov V, Aryasetiawa n F and Lichtenstein A 1997 *J. Phys.: Condens. Matter* **9** 767
[33] Petukhov A G, Mazin I I, Chioncel L and Lichtenstein A I 2003 *Phys. Rev.* B **67** 153106